Appl. Phys. 16, 211—223 (1978)

Applied Physics

Surface Polaritons in Semi-Infinite Crystals

G. Borstel

Fachbereich 4 der Universität Osnabrück, D-4500 Osnabrück, Fed. Rep. Germany

H. J. Falge

Sektion Physik, Universität München (Lehrstuhl Prof. Dr. J. Brandmüller), D-8000 München, Fed. Rep. Germany

Received 2 November 1977/Accepted 13 February 1978

Abstract. Recent progress in the field of optical surface modes in semi-infinite crystals is reviewed. The basic equations for surface polaritons originating from phonons, plasmons, excitons and magnons are given. Their observation by ATR, the resulting information and possible applications are discussed.

PACS: 63.78

In the lossless limit, surface polaritons occur at the interface between two media, one having a negative dielectric or magnetic permeability and the other a positive one. Surface polaritons propagate along the interface and decay exponentially for directions normal to the interface.

Depending on the physical mechanism responsible for the negative permeability, surface polaritons may be divided into surface phonon-, surface plasmon-, surface exciton-, and surface magnon polaritons. In addition to these pure surface states, there may occur coupled surface modes especially of the plasmon-phonon type in semiconductors. With the exception of surface magnons arising from optical modes in the *IR* spectral range, all these surface excitations so far have been observed experimentally.

Several experimental methods for studying surface polaritons have been developed in recent years. All types of surface polaritons can be observed by the methods of attenuated total reflection (ATR). In addition, coupling of an *IR* beam to the surface excitation via periodic gratings, Raman scattering and low-energy electron loss spectroscopy have been applied successfully to the observation of surface modes. This review gives a survey on the basic aspects of the different types of surface polaritons propagating at plane interfaces. For small spheres and cylinders we refer to [1, 2]. The review covers the literature up to Fall of 1977. With regard to experimental techniques, special emphasis is laid upon ATR since up to now it seems to be the most efficient method for the detection of surface polaritons. Extensions of the theory especially with regard to damping processes were discussed in [3–5].

1. General Properties of Surface Polaritons

The basic aspects of surface polaritons are most easily demonstrated for the case of a single interface. Let a semi-infinite dielectric medium (a) with dielectric constant ε_a occupy the upper half space $z>0$. The lower half space $z<0$ is filled by a second dielectric medium (b) characterized by an isotropic frequency dependent dielectric function $\varepsilon_b(\omega)$.

Solving the wave equation

$$\nabla\times\nabla\times\boldsymbol{E}+(1/c^2)\partial^2\boldsymbol{D}/\partial t^2=0 \tag{1}$$

together with the constitutive relation relating the macroscopic electric field $\boldsymbol{E}$ and the dielectric displacement field $\boldsymbol{D}$

$$\boldsymbol{D}=\varepsilon\boldsymbol{E} \tag{2}$$

in both media and imposing the usual boundary conditions for $z=0$, it is found

$$\boldsymbol{E}_{a,b}=E_0(1,0,-k_x/k_{za,b})\cdot\exp[\mathrm{i}(k_x x+k_{za,b}z-\omega t)], \tag{3a}$$

$$\boldsymbol{H}_{a,b}=(\omega/c)E_0(0,\varepsilon_{a,b}/k_{za,b},0)\cdot\exp[\mathrm{i}(k_x x+k_{za,b}z-\omega t)], \tag{3b}$$

0340-3793/78/0016/0211/$02.60

where the wave vectors $\boldsymbol{k}_{a,b}$ are given by $\boldsymbol{k}_{a,b} = (k_x, 0, k_{za,b})$ with

$$k_x^2 = (\omega^2/c^2)\varepsilon_a\varepsilon_b/(\varepsilon_a+\varepsilon_b) \tag{4a}$$

and

$$k_{za,b} = \pm(\varepsilon_{a,b}\omega/c)(\varepsilon_a+\varepsilon_b)^{-1/2}. \tag{4b}$$

From (3) it is seen that surface polaritons on isotropic dielectric media are transverse magnetic (TM) polarized waves. Equation (4a) represents the dispersion relation. The attenuation constants $\alpha_{a,b} \equiv ik_{za,b}$ of the surface wave in both media are determined by (4b). As in the lossless limit $\alpha_{a,b}$ must be real and hence $k_{za,b}$ pure imaginary, surface modes exist in the frequency region where $\varepsilon_b(\omega) \leqq -\varepsilon_a$. In the unretarded limit $k_x \to \infty$ the frequency ω_s of the excitation is given by $\varepsilon_b(\omega_s) = -\varepsilon_a$.

The two interface case may be treated in an analogeous way. Such a configuration corresponds for example to a semiconductor film (b) with thickness L epitaxically grown on an insulating substrate (c) and covered with air (a), or a thin plate (b) covered on both sides with air ($a=c$).

The dispersion relation for this case is given implicitely by [6]

$$\frac{(\varepsilon_a k_{zb}-\varepsilon_b k_{za})(\varepsilon_c k_{zb}-\varepsilon_b k_{zc})}{(\varepsilon_a k_{zb}+\varepsilon_b k_{za})(\varepsilon_c k_{zb}+\varepsilon_b k_{zc})} = \exp(2ik_{zb}L), \tag{5}$$

where

$$k_{zj} = \pm(\omega^2/c^2\varepsilon_j - k_x^2)^{1/2}, \quad j=a,b,c. \tag{6}$$

We note, as expected, that when $L \to \infty$ (5) reduces to

$$k_{za}/k_{zb} = \varepsilon_a/\varepsilon_b, \quad k_{zc}/k_{zb} = \varepsilon_c/\varepsilon_b, \tag{7}$$

which are the corresponding relations for the single interface configuration, cf. (4b).

In the symmetrical case of a plane slab with thickness L (5) results in the well known relations [7]

$$\varepsilon_b = \varepsilon_a(k_{zb}/k_{za})\tanh(ik_{zb}L/2), \tag{8a}$$

$$\varepsilon_b = \varepsilon_a(k_{zb}/k_{za})\coth(ik_{zb}L/2), \tag{8b}$$

representing odd and even parity solutions with respect to the mirror plane $z=0$.

Surface polaritons at anisotropic dielectric media exhibit a number of new phenomena not occurring on isotropic samples. In the single interface configuration of an anisotropic dielectric medium (b) with dielectric tensor $\boldsymbol{\varepsilon}_b(\omega)$ and covered with an isotropic dielectric medium (a), the surface modes in general are no longer pure TM modes but have mixed polarization TM + TE (TE: transverse electric). The analysis shows [3] that for the existence of TM surface excitations on orthorhombic samples, one principal axis of the dielectric tensor $\boldsymbol{\varepsilon}_b$ must be parallel to the interface and perpendicular to the direction of propagation of the surface wave. For such special crystal cuts the dispersion of the surface excitation is given by [3]

$$k_x^2 = \omega^2/c^2\varepsilon_a \frac{\varepsilon'_{xb}\varepsilon'_{zb}-\varepsilon_a\varepsilon_{zb}}{\varepsilon'_{xb}\varepsilon'_{zb}-\varepsilon_a^2}, \tag{9}$$

where $\varepsilon'_{xb}, \varepsilon'_{zb}$ denote principal components of $\boldsymbol{\varepsilon}_b$, and ε_{zb} the component of $\boldsymbol{\varepsilon}_b$ normal to the interface. In the static limiting case $k_x \to \infty$ one obtains from (9)

$$\varepsilon'_{xb}\varepsilon'_{zb} - \varepsilon_a^2 = 0 \tag{10}$$

which is independent of the crystal cut.

If the crystal is cut perpendicular to a dielectric principal axis we have $\varepsilon'_{zb} = \varepsilon_{zb}$, and from (9) [8]

$$k_x^2 = \omega^2/c^2\varepsilon_a\varepsilon'_{zb}\frac{\varepsilon'_{xb}-\varepsilon_a}{\varepsilon'_{xb}\varepsilon'_{zb}-\varepsilon_a^2}, \tag{11}$$

which for isotropic samples ($\varepsilon'_{xb} = \varepsilon'_{zb} = \varepsilon_b$) yields relation (4a) again.

A further characteristic property of anisotropic samples is the existence of photon-induced excitation surface modes [9, 10], i.e. solutions of (9) which occur only for a limited range of k_x values. The analysis shows [3] that the longitudinal and transverse parts of such a surface wave outside this range disintegrate into pure longitudinal and pure transverse bulk waves.

The fact that surface excitations on dielectric anisotropic media, in general, show mixed polarization TM + TE and hence ellipticity, furthermore leads to the occurence of so-called pseudo-surface polaritons. It turns out that surface excitations on such media are no longer described by the simple ansatz (3) with only one attenuation constant $\alpha_b = ik_{zb}$ inside the sample but that two constants α_{1b}, α_{2b} and hence a superposition of two particular waves is required for a proper matching of the excitations at the interface. For a bonafide surface excitation, α_{1b} and α_{2b} should be real but there are situations where α_{2b} becomes pure imaginary while α_{1b} remains real. Under these circumstances the excitation is bound to the interface via its first component but loses energy because of radiation damping of its second component. It is obvious that such a type of excitation requires a careful inclusion of damping into the theory [3].

The two interface configuration for anisotropic dielectric samples so far has been treated only for the simplest case where the dielectric principal systems of all media are parallel, and in addition, the normal to the interfaces as well as the direction of propagation of the wave coincide with a dielectric principal direction. For this special geometry the surface excitations are TM polarized. The dispersion is described by

$$\frac{(\varepsilon'_{xa}k_{zb}-\varepsilon'_{xb}k_{za})(\varepsilon'_{xc}k_{zb}-\varepsilon'_{xb}k_{zc})}{(\varepsilon'_{xa}k_{zb}+\varepsilon'_{xb}k_{za})(\varepsilon'_{xc}k_{zb}+\varepsilon'_{xb}k_{zc})} = \exp(2ik_{zb}L), \tag{12}$$

where

$$k_{zj}=\pm\left[\frac{\varepsilon'_{xj}}{\varepsilon'_{zj}}\left(\frac{\omega^2}{c^2}\varepsilon'_{zj}-k_x^2\right)\right]^{1/2}, \quad j=a,b,c. \tag{13}$$

The results outlined above are based on the assumption that spatial dispersion and effects due to dielectric inhomogeneity may be neglected. Spatial dispersion, i.e. nonlocal optical response, means that the displacement field $\boldsymbol{D}$ at position $\boldsymbol{x}$ does not only depend on the value of the electric field $\boldsymbol{E}$ at $\boldsymbol{x}$ but also on the values of $\boldsymbol{E}$ in the vicinity of $\boldsymbol{x}$

$$\boldsymbol{D}(\boldsymbol{x},\omega)=\int d^3x'\varepsilon(\boldsymbol{x},\boldsymbol{x}',\omega)\boldsymbol{E}(\boldsymbol{x}',\omega). \tag{2'}$$

If the medium is translationally invariant so that $\varepsilon(\boldsymbol{x},\boldsymbol{x}',\omega)=\varepsilon(\boldsymbol{x}-\boldsymbol{x}',\omega)$, (2') can be Fourier transformed as

$$\boldsymbol{D}(\boldsymbol{k},\omega)=\varepsilon(\boldsymbol{k},\omega)\boldsymbol{E}(\boldsymbol{k},\omega), \tag{14}$$

i.e. in the case of a nonlocal response the dielectric function depends not only on the frequency of the propagating wave but also on its wave vector.

Spatial dispersion in general may be neglected when the frequency of the excitation is in the visible or infrared part of the spectrum and one is interested in the long wavelength limit [11]. This is the usual situation for surface modes of the phonon and plasmon type observed by light reflection or light scattering experiments. However, spatial dispersion becomes important when the frequency of the excitation is close to the fundamental edge of the crystal as it occurs for surface exitons. We will return to this point in more detail in Sec. 6.

If nonlocal effects are neglected, (2') becomes

$$\boldsymbol{D}(\boldsymbol{x},\omega)=\varepsilon(\boldsymbol{x},\omega)\boldsymbol{E}(\boldsymbol{x},\omega). \tag{2''}$$

The dielectric relation is now local but ε may vary for every position $\boldsymbol{x}$ due to inhomogeneities of the material. Such situation is typical for doped semiconductors like n-InSb which contain a depletion region near the surface wherein the number of free charge carriers is reduced compared to the bulk. The analysis shows [12] that a depletion layer affects the dispersion curve only for large values of the wave vector. This range is difficult to observe by ATR and the usual approximation of ε to be uniform and equal to the bulk value up to the surface is thus reasonable.

So far we have excluded the case of an external static magnetic field acting on the dielectric media. This restriction enabled us to treat ε as a symmetric tensor which, for orthorhombic crystals and those of higher symmetry, becomes diagonal in the system of crystallographic principal axes. This property of ε would remain valid even in the presence of damping processes which have been neglected throughout this chapter. If an external static magnetic field H_s is applied, the dielectric medium shows uniaxial or lower symmetry with ε fulfilling

$$\varepsilon_{ik}(H_s)=\varepsilon_{ki}(-H_s). \tag{15}$$

In the lossless limit ε will be hermitean

$$\varepsilon_{ik}=\varepsilon_{ki}^*. \tag{16}$$

Dielectrics which show a significant effect of H_s on ε are called gyrodielectrics. With respect to surface excitations, important gyrodielectrics are doped semiconductors and metals in external magnetic fields. The most striking effect occurring in such substances is a nonreciprocal behaviour, i.e. the dispersion curves for surface modes propagating along $+x$ and along $-x$ are different, cf. Sec. 4.

In writing down (1) it was assumed that the dielectric media are nonmagnetic. The effect of a static magnetic permeability μ_j can be taken into account relatively easily, resulting in slightly more complicated dispersion relations. For example, (4a) for the single interface configuration now has the form

$$k_x^2=\frac{\omega^2}{c^2}\,\frac{\varepsilon_a^2\varepsilon_b\mu_b-\varepsilon_b^2\varepsilon_a\mu_a}{\varepsilon_a^2-\varepsilon_b^2}. \tag{4a'}$$

For dielectrics, such a generalization usually is not very important as the approximation $\mu_a\approx 1$, $\mu_b\approx 1$ is reasonable, in general.

The situation changes completely when the magnetic permeability shows dispersion, i.e. $\mu=\mu(\omega)$. As Maxwell's equations and the boundary conditions are invariant under the exchange operations $\boldsymbol{E}\to\boldsymbol{H}$, $\varepsilon\to\mu$ and $\omega\to-\omega$, surface excitations may occur also at the interface between magnetic substances or dielectric and magnetic substances, provided $\mu(\omega)$ is negative in some frequency region. Important examples of such systems are the ferri- or antiferromagnetic insulator and the ferromagnetic insulator in an external magnetic field. As these magnetic systems exhibit a strong effect of the magnetic field on $\mu(\omega)$ and hence are gyromagnetic materials, the corresponding dispersion relations become more complicated compared to dielectric systems. We shall discuss these magnetic configurations in more detail in Sec. 7.

2. Experimental Methods

The dispersion of surface polaritons on insulators and conducting materials has been investigated successfully by the ATR method. In Fig. 1 a dispersion curve (A') of surface phonon polaritons is displayed as it is calculated by (4a) for the boundary air-crystal. TM polarized radiation which is incident on a semi-infinite crystal can not interact with the surface modes.

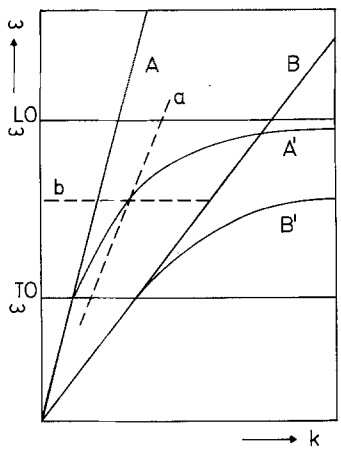

Fig. 1. Dispersion of surface phonon polaritons. A, A', B, B', a, b: see text. ω_{TO} and ω_{LO} are the frequencies of transverse and longitudinal optical bulk phonons

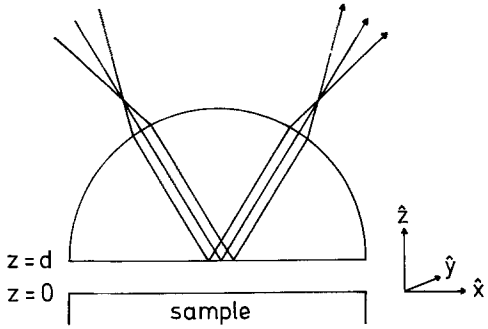

Fig. 2. Experimental arrangement

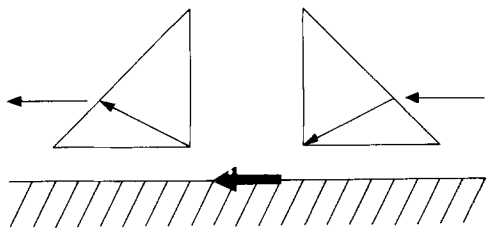

Fig. 3. Arrangement for the double prism measurement of the propagation length of surface waves [15]

Depending on the angle of incidence α one measures a reflectivity spectrum for wave vectors and frequencies which lie in the (ω, k) diagram to the left of the dispersion of light in air (A). This limitation is overcome by a modification of the well known ATR method [13]. At the base plane of a prism or hemicylinder (Fig. 2), the radiation is totally reflected when the angle of incidence exceeds the critical angle. In this case an evanescent wave exists behind the base plane. Its wave vector in x direction is given by $k=(\omega/c)n\sin\alpha$ with n being the refractive index of the hemicylinder material. Now the experimental accessible range extends in the (ω, k) diagram to the left of line B. The wave vectors corresponding to B are determined by the refractive index of the hemicylinder and the highest experimentally possible value of α. Frequency scans at fixed angle of incidence yield spectra recorded along line a. Angle scans at fixed frequency correspond to spectra recorded along line b. Resonance at the intersection of lines a or b and the dispersion curve A' may occur only when an air gap (Fig. 2: d) is left between the hemicylinder and the sample. If the sample is brought into direct contact with the hemicylinder the surface waves propagate in these two materials and the refractive index n enters in (4a). The dispersion curve A' for the boundary air—sample then is replaced by the dispersion curve B'. Obviously, no resonance can occur under these conditions. The air gap which may be filled with an appropriate dielectric is the essential point of the method. Its thickness is on the order of the wavelength of the light.

The situation is changed when a slab is investigated instead of a semi-infinite sample. In [14], the slab is brought into direct contact with the hemicylinder. For this configuration of two interfaces one of the two branches, calculated with (5), falls into the experimental accessible range.

The choice of material of the hemicylinder depends upon its transmission in the different spectral ranges and upon its refractive index. According to the polarization of surface magnon polaritons, these modes should be observable using TE polarization for the incident radiation.

The prism coupling technique is used in two other types of experiments concerning surface waves. As it is shown in Fig. 3, two prisms are applied for the investigation of the propagation length of surface waves [15]. This experiment will be described in Sec. 8. The output prism may be used only when the surface waves are excited by optical mixing of two laser beams [16]. Results of this method were reported in [17] where, however, the surface modes are detected by coherent scattering at a probe beam.

Wave vectors of the incident radiation to the right of line A in the (ω, k) diagram may be achieved by a second optical method. A periodic grating with grating spacing d is ruled in the surface of the sample. The lines are perpendicular to the plane of incidence. Near the surface, the electromagnetic field of the incident radiation is disturbed by the grating and exhibits wave vector components parallel to the surface $k_m=(\omega/c)\sin\alpha+m(2\pi/d)$ with $m=0, \pm1, \pm2, \ldots$ at the frequency of the incident radiation. The mechanically produced grating may be replaced by ultrasonic surface waves which act as a dynamic grating [18].

With Raman scattering, surface polaritons so far are only observed by forward scattering at slabs [19]. The backward scattering intensity of surface modes at one

or two interfaces has turned out to be very weak [20].

Surface polaritons with wave vectors to the right of line B in Fig. 1 are investigated by inelastic electron scattering. For summaries of this method we refer to [21, 22].

3. Surface Phonon Polaritons

The dielectric tensor for insulating crystals with orthorhombic or higher symmetry, in the lossless limit, can be written generally in the form [23]

$$\varepsilon'_\alpha(\omega)=\varepsilon_\alpha^\infty \prod_i \frac{(\omega_{\alpha i}^{LO})^2-\omega^2}{(\omega_{\alpha i}^{TO})^2-\omega^2}. \tag{17}$$

Herein $\alpha=x,y,z$ denotes the crystallographic principal directions, $\varepsilon_\alpha^\infty$ the high frequency dielectric constant and $\omega_{\alpha i}^{LO}, \omega_{\alpha i}^{TO}$ the frequencies of pure longitudinal and pure transverse phonon modes, respectively.

An alternative form for $\varepsilon'_\alpha(\omega)$ is

$$\varepsilon'_\alpha(\omega)=\varepsilon_\alpha^\infty+\sum_i \frac{4\pi\varrho_{\alpha i}(\omega_{\alpha i}^{TO})^2}{(\omega_{\alpha i}^{TO})^2-\omega^2}, \tag{18}$$

where $4\pi\varrho_{\alpha i}$ is the oscillator strength of the mode. In the case of a diatomic cubic crystal, (18) reduces to

$$\varepsilon(\omega)=\varepsilon^\infty+\frac{\varepsilon^0-\varepsilon^\infty}{1-(\omega/\omega^{TO})^2}, \tag{19}$$

with $\varepsilon^0\equiv\varepsilon(\omega=0)$.

The first experimental observation of a surface phonon polariton has been performed in 1971 by Bryksin et al. [24] for a thick NaCl plate ($L\approx 3$ mm) by means of the ATR method. Measurements of surface phonon polaritons on anisotropic samples were reported by the same authors in 1972 for uniaxial MnF_2 and TiO_2 [25].

Figure 4 shows the dispersion curve of the surface phonon polariton in GaP [26]. The solid line was calculated from (4a) and (19). Starting at $\omega=\omega^{TO}$, the branch approaches in the limiting case $k_x\to\infty$ the frequency ω_s given by

$$\omega_s=\left(\frac{\varepsilon^0+\varepsilon_a}{\varepsilon^\infty+\varepsilon_a}\right)^{1/2}\omega^{TO}. \tag{20}$$

As an example for surface phonons on more complicated crystals, Fig. 5 shows the dispersion of surface and pseudo-surface phonon polaritons on α-quartz [27]. The corresponding ATR spectra are shown in Fig. 6. The crystal cut, the direction of propagation of the mode and the frequency range under investigation where chosen to allow for the appearance of a photon-induced excitation surface mode (b) and a pseudo-surface wave (c), in addition to the usual surface phonon (a).

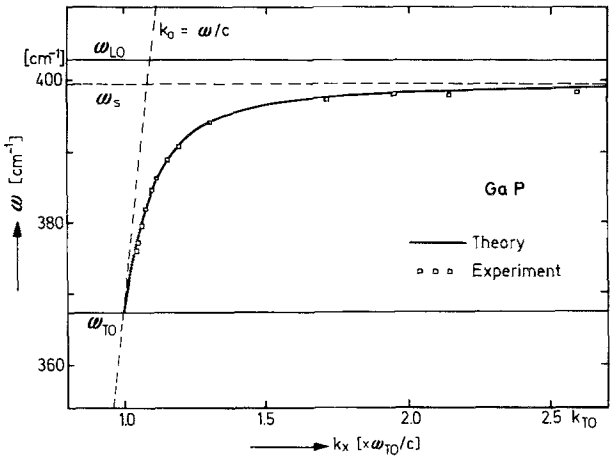

Fig. 4. Dispersion of surface phonon polaritons in GaP [26]

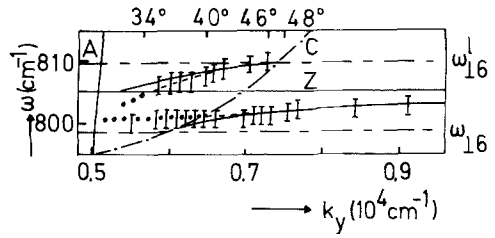

Fig. 5. Calculated and observed dispersion of surface phonon polaritons on α-quartz [27]. I: experimental values. Curved solid lines: calculated dispersion (without damping). ---: calculated dispersion (damping included). · · ·: calculated dispersion (damping included) of pseudo-surface phonon polaritons

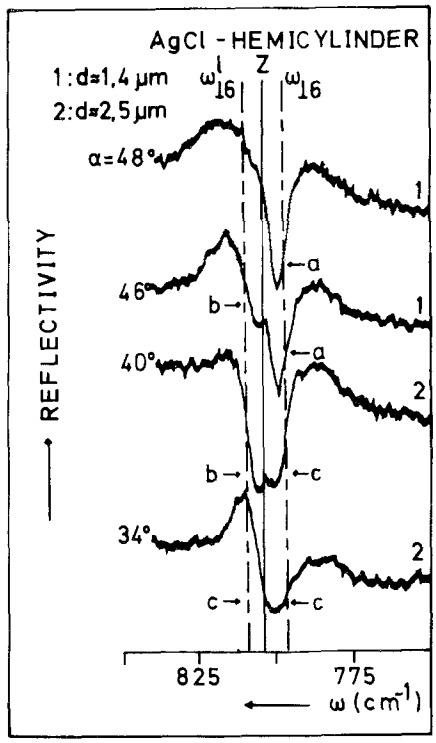

Fig. 6a–c. Spectra of surface phonon polaritons in Fig. 5 [27]. (a) Real excitation surface phonon polariton, (b) photon-induced surface phonon polariton, (c) pseudo surface phonon polariton

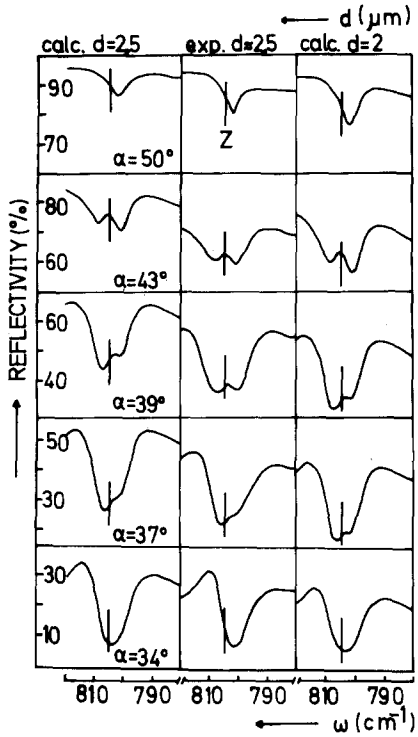

Fig. 7. Comparison of calculated and measured spectra of surface phonon polaritons in Fig. 5 [27]

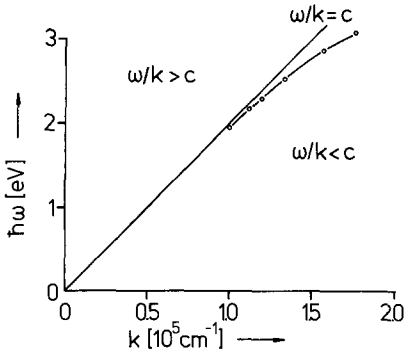

Fig. 8. Dispersion of the surface plasmon at a silver-air interface [13]

A great advantage of the ATR method is the fact that it may be treated easily theoretically, allowing for the simulation of the actual experiment on a computer. Figure 7 shows the results of such a procedure together with some experimental data of Fig. 6. For details of the calculation and specific problems connected with the inclusion of damping into the theory we refer to [3].

There exist now numerous experimental data on surface phonon polaritons in a wide range of dielectric materials. The spectroscopy of surface phonons turned out to be an efficient method to determine phonon frequencies and damping parameters in complicated crystals very accurately. For review articles especially devoted to surface phonon polaritons the reader is referred to [2, 3, 22, 28, 29].

4. Surface Plasmon Polaritons

Surface excitations on metals have been known since 1941 when Fano [30] showed Wood's anomalies on metal gratings [31] to be caused by surface plasmons.

For a free electron metal the dielectric function in the lossless limit is given by

$$\varepsilon(\omega)=1-(\omega_p/\omega)^2, \tag{21}$$

where ω_p is the plasma frequency. Combining (4a) and (21) we get for the dispersion relation of the surface plasmon in the single interface configuration

$$k_x^2=\frac{\omega^2}{c^2}\varepsilon_a\frac{\omega^2-\omega_p^2}{(\varepsilon_a+1)\omega^2-\omega_p^2}. \tag{22}$$

It is seen that surface plasmons exist in the frequency region from $\omega=0$ to $\omega=\omega_s$ where

$$\omega_s=(\varepsilon_a+1)^{-1/2}\omega_p. \tag{23}$$

For copper ($\omega_p=6.51\cdot10^4\,\mathrm{cm}^{-1}$) bounded by air ($\varepsilon_a=1$) (23) yields $\omega_s=4.6\cdot10^4\,\mathrm{cm}^{-1}$ or $\lambda_s=2172\,\text{Å}$. Thus surface plasmons in principle should be observable from the far infrared up to the near ultraviolett part of the spectrum.

The first direct observation of a surface plasmon by ATR was reported in 1968 by Otto [13] for silver. Figure 8 shows the dispersion of the surface plasmon in Ag [13]. The solid line was calculated from (22).

If damping is included via the carrier relaxation time τ the dielectric function takes the form

$$\varepsilon(\omega)=1-\frac{\omega_p^2}{\omega(\omega+i/\tau)}. \tag{24}$$

Fitting theoretical ATR spectra of surface plasmons to experimental ones may then serve as a precise method to determine optical constants of metals [32].

The observation of surface plasmons in the two interface configuration furthermore allows for studying metallic film structures and very thin coatings on metals. Thus various applications of surface mode spectroscopy in the study of adsorbates, catalysis and corrosion may be anticipated [33]. The study of depletion and accumulation layers in nonpolar semiconductors may be included here as for such materials (21) simply may be replaced by

$$\varepsilon(\omega)=\varepsilon^\infty[1-(\omega_p/\omega)^2], \tag{25}$$

where ε^∞ denotes the high frequency dielectric constant.

As mentioned before, observation of surface polaritons is also possible via coupling of light to the surface excitation by means of optical gratings or, more generally, by surface roughness. If the mode is excited

by ATR, it is thus possible to study the surface roughness spectrum. Corresponding experiments show [34] that with increasing roughness the frequency is shifted to lower values. For a quantitative measurement of the roughness spectrum we refer to [35], more recent theoretical aspects are treated in [36].

Magneto-optical studies of surface plasmons on metals and nonpolar semiconductors in dc magnetic fields yield new information on the excitation spectrum of solids. The theory of surface plasmons in magnetic fields has been developed since 1972. Metals are discussed in [37], nonpolar semiconductors which in magnetic fields show different effects are treated in [38]. In the following we shall summarize some of the results for semiinfinite samples.

Generally in such gyrodielectric media, the orientation of the static magnetic induction B_s relative to the sample normal z and the direction of propagation x of the surface plasmon is important. The three main configurations used so far in experimental studies are the Faraday case $B_s \| z$, the Voigt case $B_s \perp z$, $B_s \perp x$, and the case where $B_s \perp z$, $B_s \| x$.

For metals, an extensive discussion of all three configurations is given in [37], the results of which are reported here. In the Faraday case the surface plasmon shows mixed polarization TM + TE due to the cyclotron motion of the electrons. The dispersion is strongly affected by B_s. For a metal bounded by air ($\varepsilon_a = 1$) the surface plasmon frequency in the limit $k_x \to \infty$ is shifted from $\omega_s = \omega_p/\sqrt{2}$ [cf. (23)] to $\omega_s = (\omega_p^2 + \omega_c^2)^{1/2}/\sqrt{2}$. Herein ω_c denotes the cyclotron frequency. Furthermore the beginning of the dispersion branch is no longer at $\omega = 0$ but at $\omega = \omega_c$. This is due to the fact that a magnetic field allows for the propagation of helicon waves in the range $\omega < \omega_c$, so that localized surface modes can not exist.

For the Voigt case, the surface excitations remain TM polarized when the magnetic field is applied. This case is thus more easy to handle by ATR as ellipticity of the reflected beam is zero. The configuration exhibits nonreciprocity: Two dispersion branches of surface plasmons are found corresponding to wave propagation in $+x$ and $-x$ direction. Starting at $\omega = 0$, these branches approach in the static limit $|k_x| \to \infty$ the frequencies $\omega_{s\pm}$ given by

$$\omega_{s\pm} = (\omega_p^2/2 + \omega_c^2/4)^{1/2} \mp \omega_c/2 . \tag{26}$$

In the third configuration $B_s \perp z$, $B_s \| x$ the surface plasmons have mixed polarization again. The dispersion branch starts at $\omega = 0$ and approaches in the limit $k_x \to \infty$ the same frequency as in the Faraday case, i.e. $\omega_s = (\omega_p^2 + \omega_c^2)^{1/2}/\sqrt{2}$.

The dispersion curves for all three configurations are sketched in Fig. 9. If ε_a is increased, the limiting

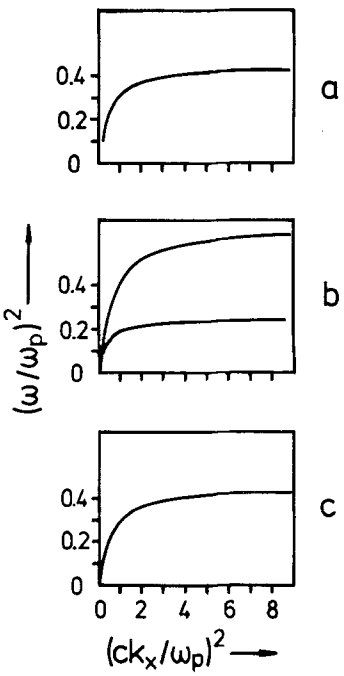

Fig. 9a–c. Dispersion of magneto-plasmon surface waves at metals [37]. (a) Faraday configuration, (b) Voigt configuration, upper branch: $k_x < 0$, lower branch: $k_x > 0$, (c) Configuration $B_s \perp z$, $B_s \| x$

frequencies for $k_x \to \infty$ decrease. In the first and third case they approach ω_c, in the second one the upper branch goes to ω_c, the lower one to zero. It must be emphasized, however, that the results outlined here are valid only for $\omega_c \ll \omega_p$ which is the usual situation in metals. If ω_c becomes comparable with ω_p the situation changes drastically. For example in the Faraday case for $\omega_c/\omega_p = 1.5$ a surface plasmon may not exist anymore [39].

In nonpolar semiconductors the situation becomes rather intricate as now $\varepsilon^\infty > 1$ and ω_c may be comparable to ω_p. The dispersion curves of magneto-plasmons so far have been discussed only for definite samples like n-InSb ($\varepsilon^\infty = 15.68$) since more general conditions for the existence of surface excitations are difficult to obtain. Though n-InSb is polar ($\omega^{TO} = 181\,\mathrm{cm}^{-1}$, $\omega^{LO} = 192\,\mathrm{cm}^{-1}$), the coupling of magneto-plasmons and phonons may be neclected provided the carrier density n is large enough ($n \gtrsim 10^{18}\,\mathrm{cm}^{-3}$), as then ω_p is well above ω^{LO}.

The dispersion curves of magneto-plasmons in n-InSb have been discussed in [39] for all three magnetic principal configurations. Compared to metals, new features are the occurence of photon-induced surface excitations, pseudo surface waves and the appearance of a gap in the dispersion relation for the Voigt case. Figure 10 shows the dispersion branches of magneto-plasmons on n-InSb for the Voigt configuration with $\omega_c/\omega_p = 0.5$ [39]. Corresponding ATR experiments are reported in [40], but the agreement between theory

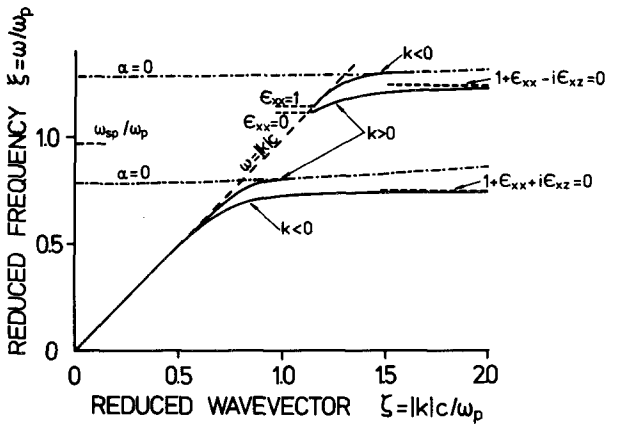

Fig. 10. Dispersion of magneto-plasmon surface waves for n-InSb in the Voigt configuration [39]

and experiment was only qualitative. This indicates that the model of a spatially homogeneous dielectric medium underlying the calculations in [39] is inappropriate for n-InSb and thus inhomogeneity and nonlocal effects must be taken into account.

The influence of depletion and accumulation layers on surface plasmons in semiconductors was treated in [41] for zero magnetic field and in [42] for nonzero field. Recent calculations based on more realistic models for the charge layer indicate [84] that a depletion layer may result in the existence of a series of guided-mode branches in addition to the usual surface plasmon branch. Similarly samples with an accumulation layer may show a second dispersion branch lying above the usual surface plasmon branch. It is expected that such calculations combined with ATR experiments will give information on the free carrier profiles in charge layers.

Surface magneto-plasmons in the weak spatial dispersion region were discussed in [43] for the Faraday case. It is found that a nonlocal surface mode with frequency near the second harmonics of the cyclotron frequency (Bernstein mode) may appear in addition.

So far only magneto-plasmons at metals or semiconductor surfaces bounded by vacuum have been considered. An extension of the theory to sandwich structures formed by semiconductor-semiconductor was given very recently in [44].

5. Plasmon-Phonon-Coupling

In polar semiconductors the free negative carrier plasmon may interact with the longitudinal optical phonon. The dielectric function then is given by a linear superposition of (19) and (25) in the form

$$\varepsilon(\omega)=\varepsilon^{\infty}+\frac{(\varepsilon^{0}-\varepsilon^{\infty})(\omega^{TO})^{2}}{(\omega^{TO})^{2}-\omega^{2}}-\frac{\omega_{p}^{2}}{\omega^{2}}. \tag{27}$$

The first experiments on plasmon-phonon surface modes have been performed by Marschall et al. [45] for n-InSb by means of coupling via optical gratings. The first ATR experiments were reported by Bryksin et al. [46]. The dispersion dependence of surface plasmon-phonon modes on n-InSb with carrier concentration $n=2\cdot10^{17}\,\mathrm{cm}^{-3}$ is shown in Fig. 11 [46]. The solid lines are calculated from (4a) and (27), the dashed lines are the dispersion branches for uncoupled plasmons and phonons. Obviously the interaction of the plasmon and the longitudinal optical phonon results in a level repulsion near the crosspoint of the dispersion curves of uncoupled excitations. The same phenomenon is seen in Fig. 12 [46] where the frequencies of coupled modes have been plotted for an angle of incidence $\alpha=23°$ ($k_x\approx1.3\omega/c$ for Si prism) against the squared plasmon frequency, which is proportional to n. As expected, the strongest level repulsion occurs for $\omega_p^2/\varepsilon^{\infty}\approx(\omega^{LO})^2$. If $\omega_p\gg\omega^{LO}$, i.e. for high carrier concentrations ($n\gtrsim10^{18}\,\mathrm{cm}^{-3}$), the interaction obviously may be neglected.

If damping is included phenomenologically (27) may be written as

$$\varepsilon(\omega)=\varepsilon^{\infty}+\frac{(\varepsilon^{0}-\varepsilon^{\infty})(\omega^{TO})^{2}}{(\omega^{TO})^{2}-\omega^{2}-\mathrm{i}\Gamma\omega}-\frac{\omega_{p}^{2}}{\omega(\omega+\mathrm{i}\gamma)}. \tag{28}$$

Extracting the phonon damping parameter Γ and the electronic damping constant γ from ATR spectra, several groups found these values to be greater than expected from bulk measurements [46, 47]. These discrepancies were attributed to different selection rules for the decay of surface modes compared to bulk excitations [46], inhomogeneous carrier density and decreased mobility of the carriers near the surface [47]. The influence of depletion, accumulation and inversion layers on the ATR resonance in semiconductors was discussed in [41]. Though all these effects in ATR experiments in general are small, such investigations are expected to give information on carrier profiles, mobility and nonparabolity of the conduction bands of semiconductors near the surface.

Application of a dc magnetic field to the sample gives rise to magneto-plasmon-phonon type surface polaritons. Such experiments allow for changing the frequency of a characteristic excitation without changing the carrier concentration in the material. As in the case of magneto-plasmons on semiconductors, the coupled magneto-plasmon phonon surface modes so far have been discussed only for specific materials. Figure 13 shows dispersion curves for n-InSb in the Voigt configuration for $k_x>0$ [48]. It is seen that both dispersion curves (cf. Fig. 11) are split into two branches.

A discussion of surface magneto-plasmon phonon excitations for all three principal magnetic configurations is given in [49] for GaAs.

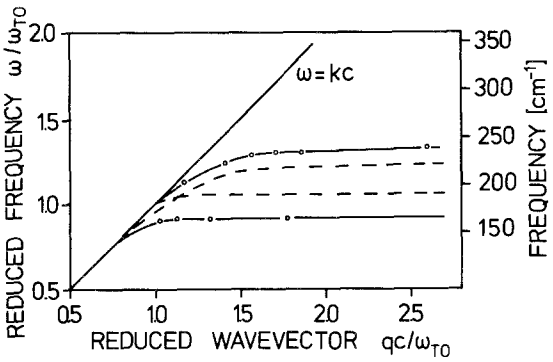

Fig. 11. Dispersion of surface plasmon-phonon modes on n-InSb for $n=2\cdot10^{17}\,\mathrm{cm}^{-3}$ [46]

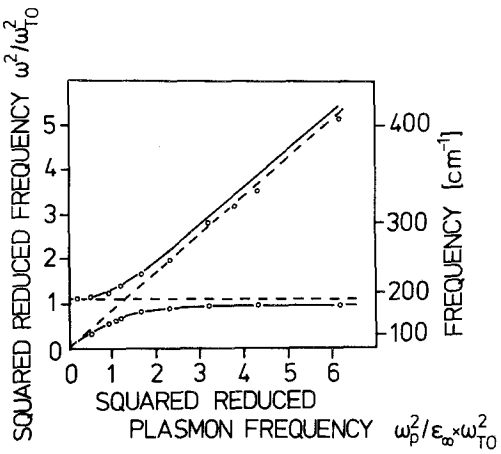

Fig. 12. Dependence of squared reduced surface plasmon-phonon frequency on squared reduced plasmon frequency [46]

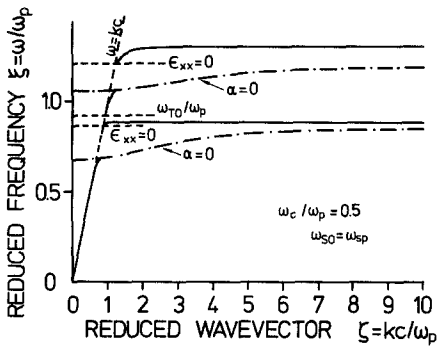

Fig. 13. Dispersion curves of magneto-plasmon-phonon surface waves for n-InSb in the Voigt configuration [48]

The first experimental study of coupled magneto-surface polaritons by ATR was reported by Palik et al. [50] for n-InSb for the geometry $B_s \perp z$, $B_s \| x$. The Voigt configuration for the same material has been investigated in [51]. As in the case of surface magneto-plasmons on semiconductors, measured ATR spectra so far could be correlated only qualitatively to the calculated dispersion curves [51]. The nonlocal shift of magneto-plasmon-phonon modes on n-InSb has been discussed recently for the unretarded limit [85].

6. Surface Exciton Polaritons

For surface excitons, in contrast to other macroscopic surface excitations, effects due to spatial dispersion are no longer negligible as now the frequency of the excitation is close to the fundamental edge of the crystal.

Since in unbounded, nonlocal or spatially dispersive media the dielectric function ε depends on the wave vector $\boldsymbol{k}$, $\varepsilon=\varepsilon(\omega,\boldsymbol{k})$, the dispersion relation $\omega=\omega(\boldsymbol{k})$ will be of higher degree in $\boldsymbol{k}$ than in the local case, resulting in the propagation of "additional" electromagnetic waves [52]. Due to the presence of additional waves for a bounded spatially dispersive medium, the usual Maxwell boundary conditions are not sufficient to determine the complete mode structure, i.e. additional boundary conditions (ABC) are required to obtain an unique solution of the boundary problem.

In earlier work it was assumed [53] that the ABC can follow only from a detailed microscopic theory of the excitation, taking into account the effects of the boundary. More recent investigations have shown, however, that such procedure is not correct. Microscopic theory must be used to derive the form of the nonlocal dielectric tensor of the medium, but once this form is explicitely specified, the ABC follows directly from the nonlocal macroscopic Maxwell's equations [54, 55].

Thus attention today is focused on the investigation of microscopic models for the bulk dielectric susceptibility χ_B, the dielectric susceptibility χ_S near the surface, and the passage from χ_B to χ_S [56, 57].

As these microscopic investigations are still in progress, the ABC used so far to calculate the dispersion and ATR response of surface excitons differ. It has been suggested [58] that experiments may elucidate the applicability of the various microscopic models but a definite decision is still lacking.

The ABC most commonly used have a form where either the polarization field (exciton ABC) or the derivative of the polarization field (plasmon ABC) vanishes at the surface $z=0$. The influence of both ABC on the surface exciton dispersion relation recently has been discussed in [59], the results of which are reported here.

For the plasmon ABC $\partial P_x(0)/\partial z=0$, which corresponds to the symmetry condition $E_x(z)=E_x(-z)$, $H_y(z)=-H_y(-z)$ originally proposed in [60], the dispersion relation for a semiinfinite sample bounded by air ($\varepsilon_a=1$) is given implicitely by

$$-(k_x^2-\omega^2/c^2)^{1/2}=\frac{2\omega^2}{\pi c^2}\int_0^\infty \frac{dk_z}{k^2}\cdot\left(\frac{k_x^2}{\omega^2/c^2\varepsilon_l}+\frac{k_z^2}{\omega^2/c^2\varepsilon_t-k^2}\right). \tag{29a}$$

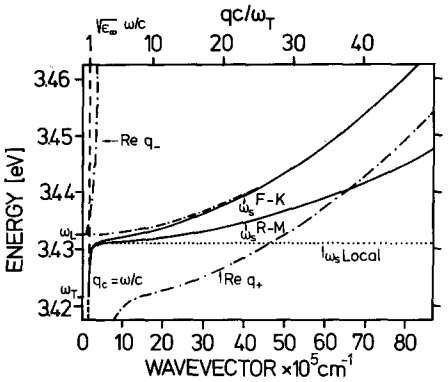

Fig. 14. Surface exciton dispersion (solid lines) in ZnO for plasmon (F–K) and exciton (R–M) ABC. Dotted line is the local surface dispersion, the dot-dash curves are the bulk polariton dispersions [59]

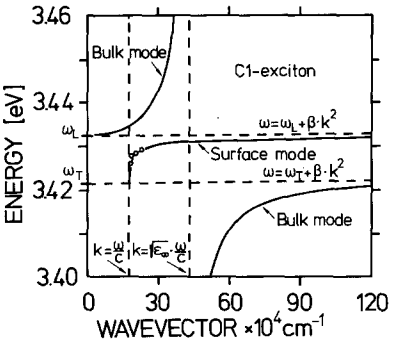

Fig. 15. Dispersion curves of surface and bulk excitons in ZnO. The solid lines are calculated; the rectangles are experimentally determined [64]

The exciton ABC $P_x(0)=0$, corresponding to $E_x(z)=-E_x(-z)$, $H_y(z)=H_y(-z)$ [61] results in

$$(k_x^2-\omega^2/c^2)^{-1/2}=\frac{2}{\pi}\int_0^\infty dk_z\frac{\varepsilon_t}{\omega^2/c^2\varepsilon_t-k^2}. \tag{29b}$$

Herein ε_t and ε_l denote the transverse and longitudinal dielectric functions which in the hydrodynamic approximation have the form

$$\varepsilon_{t,l}=\varepsilon^\infty+\frac{4\pi\varrho\omega_T^2}{\omega_T^2-\beta_{t,l}k^2-\omega(\omega+\mathrm{i}/\tau)}. \tag{30}$$

The coefficients $\beta_{t,l}$ are inverse proportional to the transverse and longitudinal effective exciton masses. In the unretarded limit, the two integrals reduce to

$$-1=\frac{2k_x}{\pi}\int_0^\infty\frac{dk_z}{k^2\varepsilon_l}, \tag{31a}$$

and

$$-1=\frac{2k_x}{\pi}\int_0^\infty dk_z\varepsilon_t/k^2. \tag{31b}$$

If the dielectric functions (30) are introduced into the integrals the integration may be carried out resulting in explicit dispersion relations. The analytic expressions are rather cumbersome and were given in [59] for (29a) and (29b), in [62] for (31a) and in [63] for (31b). For interacting excitonic resonances we refer to [86].

Figure 14 shows the surface exciton dispersion relations (solid lines) derived from (29a) and (29b) for ZnO [59]. It is seen that for the plasmon ABC the dispersion curve approaches the bulk longitudinal dispersion curve $\varepsilon_l(\omega,k)=0$. For the exciton ABC the dispersion curve rises to a maximum (not shown in Fig. 14) and in the unretarded limit $k_x\to\infty$ approaches the local limit $\varepsilon(\omega)=-1$.

The first observation of a surface exciton was reported in 1976 by Lagois and Fischer for ZnO [64]. Subsequently data on CuBr [65], ZnSe [66], and CuCl [67] have been published. Figure 15 shows the results for ZnO [64] together with the theoretical curve calculated from (29a). Comparing Figs. 14 and 15 it is seen that the range of k_x values accessible so far by ATR is too small to allow for a definite decision between the two dispersion relations (29a) and (29b). This experimental restriction stems from the lack of suitable prism materials with a large index of refraction in the visible and ultraviolett region.

A further effect of spatial dispersion on the surface exciton becomes obvious from a comparison of Figs. 4 and 14. In Fig. 4, a clear gap for bulk excitations exists between ω^{TO} and ω^{LO} which prevents energy stored in the surface excitation from leaking into the crystal's interior. In a spatially dispersive medium no gap is present (Fig. 14) and the surface polariton may leak energy into the interior of the crystal. Consequently the surface mode is damped even in a lossless dielectric medium. This contribution to the damping rate in principle may be investigated by an analysis of the ATR lineshape and corresponding studies thus might serve as a test for different ABC in model calculations [68].

7. Surface Magnon Polaritons

It is well known that magnetic crystals may exhibit optical magnons in the infrared spectral region. Examples are magnetite or yttrium-iron garnet for ferrimagnets and FeF_2 or CoF_2 for antiferromagnets. The dispersion of the bulk polaritons of these elementary excitations has not yet been investigated experimentally. Theoretical considerations are given in [69–72, 87]. Corresponding surface magnons (high-frequency surface magnons) have also not yet been measured. For low-frequency surface magnons, observable by microwave techniques, theoretical results concerning a single-interface geometry are given in [22, 73, 74]. The theoretical treatment of coupled photon surface mag-

non modes on a semi-infinite crystal is rather similar to the phenomenological treatment of surface phonon polaritons when the appropriate magnetic permeability tensor is evaluated. This applies for bulk polaritons in magnetic crystals, too [69]. Depending upon the magnetic character of the crystal and upon an applied static external magnetic field, a rich variety of bulk and surface polaritons is expected. Here we summarize the results for TE polarized surface polaritons on ferromagnetic insulators [74]. This example shows the basic properties of magnon type surface polaritons.

The geometrical arrangement is given in Fig. 16. For simplicity, the dielectric functions are assumed to be $\varepsilon_i = 1$. The dispersion of bulk polaritons propagating in the x direction with $H_z = 0$ and $E \| z$ is determined by $k = (\omega/c)\mu_v$. $\mu_v = \mu_{xx} + \mu_{xy}^2/\mu_{xx}$ is the Voigt configuration magnetic permeability function. Figure 17 shows its frequency dependence. The dispersion of the bulk magnon polaritons is displayed in Fig. 18 by the dash-dotted curves. They are symmetrical for k propagating in $+x$ and $-x$ direction. This is not the case for the dispersion (full curves) of the magnon surface modes. The nonreciprocal nature of the propagation arises because the magnetic field H of both the $+k$ and $-k$ modes rotate in the same sense according to the precession of spin waves about the static magnetic field. The polaritons which correspond to $-k$ solutions do not exist without a driving field. Furthermore, the condition $\mu_0 > 1$ has to be fulfilled. In contrast to the behavior of surface phonon polaritons, the $-k$ solutions are also propagating in a frequency region where bulk polaritons exist simultaneously. The $+k$ solution reaches, for $k \to \infty$, the frequency of unretarded surface magnons ω_{sp}. It starts at the frequency ω_v which is dependent on the external field H_0. If the dielectric permeability $\varepsilon(\omega)$ of the crystal has anomalous dispersion in the frequency range of interest, the situation becomes much more complicated. Then, for example, bulk modes exist in frequency ranges of negative $\mu(\omega)$ when $\varepsilon(\omega)$ is negative, too [75]. This seems to be the case in the infrared spectral region for many ferrimagnets [76]. The corresponding modes in semi-infinite samples should be observable by the ATR technique [77] as well as TE and TM polarized surface modes by the modified ATR method [13]. It is expected that this field will be developed in the next years.

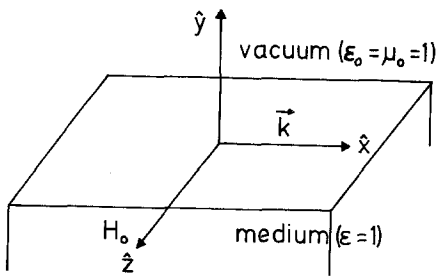

Fig. 16. Voigt geometry for surface polaritons

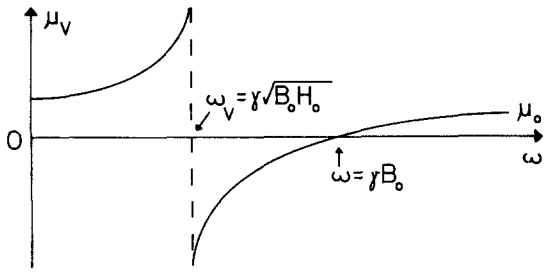

Fig. 17. Frequency dependence of magnetic permeability in the Voigt geometry [74]

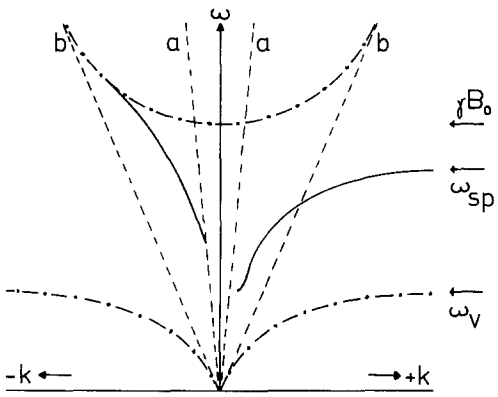

Fig. 18. Dispersion of surface polaritons for the two non-equivalent directions of propagation on a gyromagnetic medium [74]

8. Further Remarks

As it has been pointed out in the preceeding sections, the investigation of surface polaritons is in a state where many of the theoretical predictions have been confirmed experimentally. Furthermore the ATR method is useful in obtaining information about optical data of very different solids. In this context applications concerning the propagation length L of surface modes should be mentioned [15, 33, 78–81].

In [15] it has been shown that it is possible to measure the propagation length of surface polaritons by a double prism method. The experimental set-up is shown in Fig. 3. The 10.6 μm output of a 250 mW cw CO_2 laser was used as the source of input radiation which is converted into surface polaritons by the first prism. The back-convert for optical detection is maintained by the output prism. Then the intensity of the output beam, normalized to the incident radiation, is measured as a function of the distance between the two prisms. From the slope of the resulting plot the propagation length L, i.e. the distance at which the mode intensity decays to 1/e of its initial value, is

evaluated. These experiments are performed using the CO_2 laser because at the investigated metal/air interface L has appreciable higher values in the infrared than in the visible ($L < 10^{-4}$ cm). For a copper-air interface in [15], $L = 1.9$ cm has been obtained. Data for other materials are given in [70]. In the review [33] the application of this method to the study of thin films, catalysis, corrosion and other surface problems is anticipated.

Another type of application was proposed in [82]. In the region of phase transitions, the intensity of dielectric permeability fluctuations increases due to fluctuations of the order parameter. This should lead to a decrease in the propagation length of surface polaritons. The temperature dependence of the Rayleigh wave velocity, investigated in [83], confirms that acoustic surface modes are sensitive to the critical properties of a solid. It is thus expected that similar experiments in the optical range will allow to study the fluctuations of the order parameter in solids exhibiting phase transitions.

Acknowledgement. We thank Prof. Dr. J. Brandmüller for his interest in this work and Dr. R. L. Schmidt for a critical reading of the manuscript. For the financial support we are very much obliged to the "Deutsche Forschungsgemeinschaft".

References

1. R. Ruppin, R. Englman: Rep. Prog. Phys. **33**, 149 (1970)
2. K. L. Kliewer, R. Fuchs: In *Advances in Chemical Physics*, Vol. 27 (Wiley, New York 1974)
3. G. Borstel, H. J. Falge: phys. stat. sol. (b) **83**, 11 (1977)
4. A. Otto: In Proc. Taormina Conf. on Polaritons, ed. by E. Burstein and F. de Martini (Pergamon Press, New York 1974), p. 117
5. G. N. Zhizhin, M. A. Moskalewa, V. G. Nazin, V. A. Yakovlev: Fiz. Tverd. Tela **19**, 1309 (1977)
6. E. Burstein, A. Hartstein, J. Schoenwald, A. A. Maradudin, D. L. Mills, R. F. Wallis: In Proc. Taormina Conf. on Polaritons, ed. by E. Burstein and F. de Martini (Pergamon Press, New York 1974), p. 89
7. K. L. Kliewer, R. Fuchs: Phys. Rev. **144**, 495 (1966)
8. A. Hartstein, E. Burstein, J. J. Brion, R. F. Wallis: Surf. Sci. **34**, 81 (1973)
9. O. A. Dubovskii: Fiz. Tverd. Tela **12**, 3054 (1970) [Sov. Phys.—Solid State **12**, 2471 (1971)]
10. A. Hartstein, E. Burstein, J. J. Brion, R. F. Wallis: In Proc. Taormina Conf. on Polaritons, ed. by E. Burstein and F. de Martini (Pergamon Press, New York 1974), p. 111
11. A. A. Maradudin, D. L. Mills: Phys. Rev. B **7**, 2787 (1973)
12. S. L. Cunningham, A. A. Maradudin, R. F. Wallis: Phys. Rev. B **10**, 3342 (1974)
13. A. Otto: Z. Physik **216**, 398 (1968)
14. E. Kretschmann: Z. Physik **241**, 313 (1971)
15. J. Schoenwald, E. Burstein, J. M. Elson: Solid State Commun. **12**, 185 (1973)
16. F. de Martini, Y. R. Shen: Phys. Rev. Lett **36**, 216 (1976)
17. F. de Martini, G. G. Giuliani, P. Mataloni, E. Palange, Y. R. Shen: 9th Int. Conf. on Quantum Electronics, Amsterdam (1976)
18. J. Schoenwald, E. Burstein, R. F. Wallis: Bull. Am. Phys. Soc. **16**, 1409 (1972)
19. D. J. Evans, S. Ushioda, J. D. McMullen: Phys. Rev. Lett. **31**, 369 (1973)
20. Y. J. Shen, E. Burstein, D. L. Mills: Phys. Rev. Lett. **34**, 1516 (1975)
21. A. Otto: In *Festkörperprobleme*, Vol. XIV, ed. by H. J. Queisser, (Vieweg, Braunschweig 1974), p. 1
22. V. V. Bryksin, D. N. Mirlin, Yu. A. Firsov: Usp. Fiz. Nauk. **113**, 29 (1974) [Sov. Phys.—Usp. **17**, 305 (1975)]
23. R. Claus, L. Merten, J. Brandmüller: Springer Tracts in Modern Physics, Vol. 75 (Springer, Berlin, Heidelberg, New York 1975)
24. V. V. Bryksin, Yu. M. Gerbshtein, D. N. Mirlin: Fiz. Tverd. Tela **13**, 2125 (1971) [Sov. Phys.—Solid State **13**, 1779 (1972)]
25. V. V. Bryksin, D. N. Mirlin, I. I. Reshina: ZhEFT Pis. Red. **16**, 445 (1972) [Sov. Phys.—JETP Lett. **16**, 315 (1972)]
26. N. Marschall, B. Fischer: Phys. Rev. Lett. **28**, 811 (1972)
27. E. Schuller, G. Borstel, H. J. Falge: phys. stat. sol. (b) **69**, 467 (1975)
28. G. Borstel, H. J. Falge, A. Otto: Springer Tracts in Modern Physics, Vol. 74 (Springer, Berlin, Heidelberg, New York 1974), p. 107
29. V. M. Agranovich: Usp. Fiz. Nauk. **115**, 199 (1975) [Sov. Phys.—Usp. **18**, 99 (1975)]
30. U. Fano: J. Opt. Soc. Am. **31**, 213 (1941)
31. R. W. Wood: Phys. Rev. **48**, 928 (1935)
32. A. Otto: In *Optical Properties of Solids, New Developments*, ed. by B. O. Seraphin, (North-Holland, Amsterdam 1976) p. 677
33. R. J. Bell, R. W. Alexander, Jr., C. A. Ward, I. J. Tyler: Surf. Sci. **48**, 253 (1975)
34. A. J. Braundmaier, Jr., E. T. Arakawa: J. Phys. Chem. Solids **35**, 517 (1974)
35. J. Bodesheim, A. Otto: Surf. Sci. **45**, 441 (1974)
36. A. A. Maradudin, W. Zierau: Phys. Rev. B **14**, 484 (1976)
37. K. W. Chiu, J. J. Quinn: Nuov. Cim. **10** B, 1 (1972)
38. J. J. Brion, R. F. Wallis, A. Hartstein, E. Burstein: Phys. Rev. Lett. **28**, 1455 (1972)
39. R. F. Wallis, J. J. Brion, E. Burstein, A. Hartstein: Phys. Rev. B **9**, 3424 (1974)
40. A. Hartstein, E. Burstein: Solid State Commun. **14**, 1223 (1974)
41. R. T. Holm, E. D. Palik: Crit. Rev. Solid State Sci. **5**, 397 (1975)
42. R. F. Wallis, J. J. Brion, E. Burstein, A. Hartstein: Proc. 11th Int. Conf. on Physics of Semiconductors, PWN Warschau (1972), p. 1448
43. Y. Omura, M. Tsuji: J. Phys. Soc. Japan **40**, 107 (1976)
44. C. Uberoi, U. J. Rao: Surf. Sci. **66**, 210 (1977)
45. N. Marschall, B. Fischer, H. J. Queisser: Phys. Rev. Lett. **27**, 95 (1971)
46. V. V. Bryksin, D. N. Mirlin, I. I. Reshina: Solid State Commun. **11**, 695 (1972)
47. R. W. Gammon, E. D. Palik: J. Opt. Soc. Am. **64**, 350 (1974)
48. J. J. Brion, R. F. Wallis, A. Hartstein, E. Burstein: Surf. Sci. **34**, 73 (1973)
49. J. J. Quinn, K. W. Chiu: In Proc. Taormina Conf. on Polaritons, ed. by E. Burstein and F. de Martini (Pergamon Press, New York 1974), p. 259
50. E. D. Palik, R. Kaplan, R. W. Gammon, H. Kaplan, J. J. Quinn, R. F. Wallis: Phys. Lett. **45** A, 143 (1973)
51. A. Hartstein, E. Burstein, E. D. Palik, R. Kaplan, R. W. Gammon, B. W. Henvis: Proc. 12th Int. Conf. on Physics of Semiconductors, Stuttgart (1974), p. 541
52. S. I. Pekar: Zh. Eksp. Teor. Fiz. **33**, 1022 (1957), [Sov. Phys.—JETP **6**, 785 (1958)]
53. V. M. Agranovich, V. L. Ginzburg: *Spatial Dispersion in Crystal Optics and the Theory of Excitons* (Interscience, London 1966)
54. J. J. Sein: Phys. Lett. **32** A, 141 (1970)
55. J. L. Birman, J. J. Sein: Phys. Rev. B **6**, 2482 (1972)

56. M.J.Frankel, J.L.Birman: Phys. Rev. B **13**, 2587 (1976)
57. D.L.Johnson, P.R.Rimbey: Phys. Rev. B **14**, 2398 (1976)
58. G.D.Mahan: In *Elementary Excitations in Solids, Molecules and Atoms*, ed. by J.T.Devrese, A.B.Kunz, and T.C.Collins (Plenum, New York 1974), part. B, p. 93
59. P.R.Rimbey: Phys. Rev. B **15**, 1215 (1977)
60. K.L.Kliewer, R.Fuchs: Phys. Rev. **172**, 607 (1968)
61. P.R.Rimbey, G.D.Mahan: Solid State Commun. **15**, 35 (1974)
62. B.Fischer, H.J.Queisser: Solid State Commun. **16**, 1125 (1975); Crit. Rev. Solid State Sci. **5**, 281 (1975)
63. P.R.Rimbey: phys. stat. sol. (b) **68**, 617 (1975)
64. J.Lagois, B.Fischer: Phys. Rev. Lett. **36**, 680 (1976)
65. I.Hirabayashi, T.Koda, Y.Tokura, J.Murata, Y.Kaneko: J. Phys. Soc. Japan **40**, 1215 (1976)
66. Y.Tokura, I.Hirabayashi, T.Koda: J. Phys. Soc. Japan **42**, 1071 (1977)
67. I.Hirabayashi, T.Koda, Y.Tokura, J.Murata, Y.Kaneko: J. Phys. Soc. Japan **43**, 173 (1977)
68. J.Lagois, B.Fischer: Proc. 13th Int. Conf. on Physics of Semiconductors, Rome (1976), p. 788
69. D.L.Mills, E.Burstein: Rep. Prog. Phys. **37**, 817 (1974)
70. S.Manohar, G.Venkataraman: Phys. Rev. B **5**, 1993 (1972)
71. S.M.Bose, E.Foo, M.A.Zuniga: Phys. Rev. B **12**, 3855 (1975)
72. M.I.Kaganov, N.K.T'yau: Fiz. Tverd. Tela **17**, 2857 (1975), [Sov. Phys.—Solid State **17**, 1909 (1976)]
73. J.P.Parekh, S.R.Ponamgi: J. Appl. Phys. **44**, 1384 (1973)
74. A.Hartstein, E.Burstein, A.A.Maradudin, R.Brewer, R.F.Wallis: J. Phys. C **6**, 1266 (1973)
75. V.G.Veselago: In Proc. Taormina Conf. on Polaritons, ed. by E.Burstein and F.de Martini (Pergamon Press, New York 1974) p. 5
76. A.B.Harris: Phys. Rev. **132**, 2398 (1963)
77. H.J.Falge, A.Otto, W.Sohler: phys. stat. sol. (b) **63**, 259 (1974)
78. C.A.Ward, R.J.Bell, R.W.Alexander, G.S.Kovener, I.L.Tyler: Appl. Opt. **13**, 2378 (1974)
79. C.A.Ward, R.W.Alexander, R.J.Bell: Phys. Rev. B **14**, 856 (1976)
80. G.N.Zhizhin, M.A.Moskalewa, E.V.Shomina, V.A.Yakovlev: ZhEFT Pis. Red. **24**, 221 (1976), [Sov. Phys.—JETP Lett. **24**, 197 (1976)]
81. E.Burstein, W.P.Chen, Y.J.Chen, A.Hartstein: J. Vac. Sci. Technol. **11**, 1004 (1974)
82. V.M.Agranovich, T.A.Leskova: Solid State Commun. **21**, 1065 (1977)
83. L.B.Bjerkan, K.Fossheim: Solid State Commun. **21**, 1147 (1977)
84. C.C.Kao, E.M.Conwell: Phys. Rev. B **14**, 2464 (1976)
85. J.J.Brion, R.F.Wallis, N.J.M.Horig: Surf. Sci. **65**, 379 (1977)
86. J.Lagois: Phys. Rev. B **16**, 1699 (1977)
87. E.F.Sarmento, D.R.Tilley: J. Phys. C **9**, 2943 (1976), **10**, 795 and 4269 (1977)